Check for updates

Z-Pinning Techniques to Improve Energy Absorption Capabilities of CFRP Tubular Structures

J. G. Ramírez[1] · H. Ghasemnejad[1]

Abstract

This paper investigates the use of z-pinning reinforcement in CFRP tubular structures under axial impact, to find the optimum design to increase the specific energy absorption (SEA). Through-the-thickness reinforcement is known as a technique to improve integrity and fracture resistance in composite materials and structures. Manufacturing and testing of unpinned tubular structures are conducted to create a base model to validate numerical results. A finite element model of the tube under dynamic impact is developed using LS-DYNA software, conducting parametric studies, mesh sensitivity analysis and trigger modelling research. The proposed z-pinning modelling techniques are researched, and an energy-based contact model is proposed to model pinned areas. Five different designs of reinforced tubes are designed and analysed, to find the optimum z-pinned pattern in terms of SEA. The novelties of this research indicate that z-pinning can improve the SEA and reduce the initial collapse load during crushing. Our results indicate that the vertical banded design shows the highest SEA and least initial collapse load values in comparison with the unpinned specimen, which indicates an improvement in the crashworthiness parameters of z-pinned composite tubes.

1 Introduction

Crashworthiness is defined as the ability of structural components to protect passengers during an impact event. The energy absorption capability of the material is the most important parameter for structural components [1]. In the last decades, many studies have been made to understand the ability of composite materials to absorb impact energy, especially when it comes to carbon fibre-reinforced polymer (CFRP) composite materials.

The main reason behind the high energy absorption capability of the polymer composite materials is related to brittle behaviour which causes a progressive crushing process, dominated by delamination mode I and the formation of continuous fronds or bundles in tubular structures [2]. Some studies have been made to determine the factors which affect the

---

✉ H. Ghasemnejad
    Hessam.Ghasemnejad@cranfield.ac.uk

1   Centre for Aeronautics, Cranfield University, England MK43 0AL, UK

Springer

energy absorption capability of composite tubes [2, 4], concluding that the fibre and matrix materials, laminate design, structural geometry, and trigger mechanisms are the main variables affecting the specific energy absorption (SEA).

Cauchy Savona et al. [4] concluded that higher Mode-I and Mode-II properties yield high crushing energies. Ghasemnejad et al. [5, 6] proved that SEA in axial crushing depends on the interlaminar fracture toughness with a non-linear relationship, which is due to the fact of the formation of a central inter-wall crack in Mode-I. This theory is reinforced by some other experimental studies [7-9]. Several technologies such as 3D Knitting, weaving, and braiding [10-14]; z-anchoring [15]; stitching [16-20] and z-pinning have been developed to achieve crack growth resistance.

Particularly, in terms of z-pinning, this technology consists of inserting pins in the stacking direction of the laminate. These pins can be made of metal or pre-preg laminates which have been processed, with a diameter between 0.28 and 0.51 mm [21]. Two methods are available to introduce the pins into the laminate. The first one consists of a pressure plate to insert z-pins during the standards curing cycle [21]. The other method is the Ultrasonic Assisted z-Fibre™ (UAZ™), in which the z-pins are introduced by using an ultrasonic horn before the curing. This is the most used, and it can be applied to CFRP tubular structures [21]. The interlaminar fracture toughness for z-pinned laminates has been deeply studied, especially under Mode-I and Mode-II [15, 22, 24]. It has been shown that the fracture toughness is linearly increased with the volume content of z-pins, being higher in the case of G_IC and G_IIC. The impact damage tolerance and fracture toughness properties are increased with z-pins according to Mouritz [25]. Dickson et al. [26] showed an increase of 23% in the elastic modulus in the stacking direction with a 1.9% volume content of z-pins. However, a slight reduction in the in-plane Young's modulus and strengths has been reported by Chang et al. [27], mainly attributed to the fibre breakage during the inclusion of z-pins. Lander [23] studied the effect of a rectangular pattern of z-pins on 3 different CFRP tubes of 8,12 and 16 plies. It resulted in an increase of 24%, 53% and 76% in the SEA with higher peak loads, and decelerations.

Various FEM modelling techniques of z-pinning have been used in previous studies; however, none of them has been implemented in CFRP tubes under axial crushing. Two main techniques are recognised to model z-pinning: discrete z-pin modelling and Cohesive Zone Modelling (CZM). The discrete z-pin modelling technique introduces modelling each z-pin as a discrete solid within the composite material. Generally, a solid material is used to model z-pin, with equivalent properties based on experimental testing. A bonding interface is defined between the laminate and each z-pin. These models were studied by Mengjia and Puhui [28] and have shown good results under Mode I and 30º mixed loading, although interfacial strength has shown too high values. Also, 1D truss elements have been used to model each pin, with a more efficient approach, according to Blacklock et al. [29]. This technique has shown good results in the literature even for not simple geometries as for T-joints [30]. However, this is not practical to apply this method to geometry such as CFRP tubes, since the number of z-pins which must be modelled is excessive.In a similar approach to CZM, the following research is developed to use energy-based contact definitions to define enhanced delamination properties between different shells of a reinforced laminate. As explained before, an energy-based contact model which is defined at the interface between two layers is initially bonded, and after reaching determining stress, the contact load is linearly decreased until a critical distance is reached. Liu et al. [31] investigated the effects of Z-pin content and insertion angle

on the deformation and failure of quasi-isotropic laminates in the thickness direction by tensile pull-out tests and out-of-plane tensile tests. Local defect characteristics of the composite laminates when carbon fibre pin needle arrays are inserted were reproduced to analyse the Z-pin pull-out stresses and failure mechanism. Their results demonstrate that the decrease can be attributed to the resin-rich zone defect caused by Z-pin insertion and was not significantly associated with local in-plane fibre buckling. Knapp and Scharr [32] represented the results of the investigations on in-plane compression properties of unidirectional carbon-fibre/epoxy laminates with a three-dimensional z-pin reinforcement with circumferentially notched z-pins. According to their results, Young's modulus of the z-pinned laminate is not affected by the notching of the z-pins. An influence of the notch design, depth and distance of circumferential notches on Young's modulus was not found in the investigation carried out. Liao et al. [33] investigated the low-velocity impact behaviours of $[0_2/90_2]_{4S}$ cross-ply composite laminates by inserting Z-pins with two different angles 0° and ±45° along the thickness direction were compared. Based on the mechanical characteristics, 0° Z-pinning could improve the resistance to the onset of penetration by comparing to the ±45° Z-pinning. In addition, the effectiveness of 0° Z-pinning on suppression of delamination damage and internal defects was better than the ±45° Z-pinning at high impact energy.

However, the studies on z-pinned composite tubular structures are limited. This fact defines the novelty of this research to investigate the effect of various z-pinning patterns on the energy absorption capability of composite tubular absorbers. This study aims to investigate the improvement in the energy absorption capability of CFRP tubular structures by using the z-pinning technique. Due to the high manufacturing costs of z-pinning, the numerical approach is the most convenient method to investigate different designs of z-pinning patterns in CFRP tubular structures.

2 Experimental Studies

2.1 Manufacturing of Specimens

Three unpinned CFRP tubes with 80*mm* height were manufactured to create experimental data for validation purposes. The procedure of manufacturing is based on hand layup which is wrapping each carbon/epoxy pre-impregnated ply onto an aluminium mandrel with a 90*mm* outer diameter. The carbon/epoxy (XC130 300 g Unidirectional Prepreg Carbon Fibre with a density of ρ = 1750 kg/m3 and GMS of 12 oz. per square yard) with a symmetrical 10 plies of $[-45/45/0/90/0]_s$ and a total thickness of 2.8*mm* was used in this study. After wrapping two plies, a de-bulking procedure which consists of a vacuum cycle with ultrasonic waves sent to the uncured material through an ultrasonic transducer is performed to ensure a suitable vacuuming process within the laminate. Once the tubes had been laid-up, they were placed between pre-cut aluminium plates to keep them flat during the curing process. The plates were pre-treated with a mould cleaner to remove grease and debris and a monocot wax was applied to prevent escaped epoxy from the prepreg bonding to the metal plates. The plates were then covered in non-stick polymer sheets to further decrease the chance of epoxy bonding to the plates. The plates were placed on either side of the uncured composite, then covered top and bottom with three

sheets of 'breather cloth' and placed inside a heat-resistant polymer bag. The breather cloth has the appearance of cotton wool and allows air to circulate through the bag preventing the formation of air pockets. The bagging material was cut from a roll and was opened at either end. A high-temperature, double-sided epoxy tape was used to seal the ends. Once sealed, an air suction valve is inserted through the bag and a pipe connecting the valve to a vacuum pump. The vacuum pump was used to evacuate the bag, with the aid of the breather cloth. This has the effect of pressing the aluminium plates tightly together and forcing the plies of prepreg together, allowing good adhesion between the plies and eliminating air that could cause voids in the composite. The pressure gauge was inserted via a second valve to monitor the pressure in the bag. This can be used to ensure the correct pressure is applied to the bag (following the manufacturer's guidelines). The pressure gauge was also used to measure any pressure drop in the vacuum bag once the pump had been switched off and hence to check if the bag was properly sealed. A trigger chamfer of 45° is machined in each tube. This trigger mechanism has been adopted according to the literature which gives the best energy absorption in comparison with the other angles [5, 6]. The geometry of each tube and an image of one of the samples are shown in Fig. 1. More details of the manufacturing process of composite specimens can be found in [34, 35].

2.2 Impact Testing

The impact test was conducted by using a drop tower with an impactor mass of 108.4 kg and a drop height of 2.0 m with a velocity of 7.022 m/s for all specimens. This gives the maximum kinetic energy of 2672 J. The drop mass was released from a pre-determined height to initiate and record the load against time until it reaches the impact energy of 2672 J. The hammer then is pulled up by the machine. The initial height of the hammerhead is $2m$, and the load against the time curve is recorded with a dynamic load cell recorded with an accelerometer and sampled at $200kHz$. The initial setup of the test specimen is shown in Fig. 2.
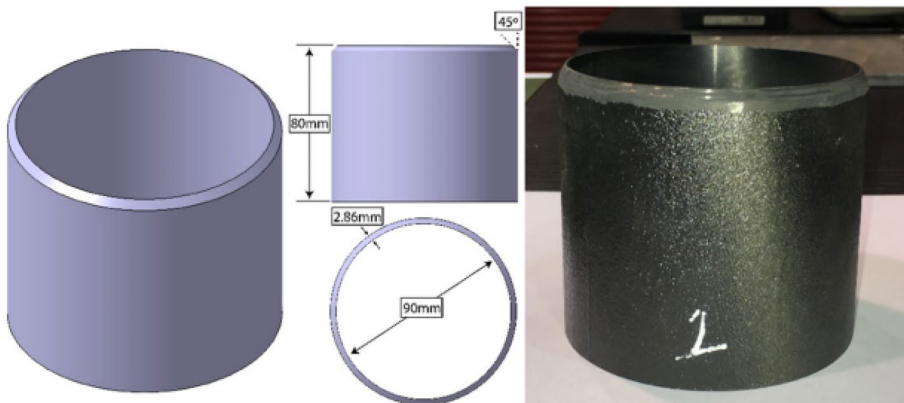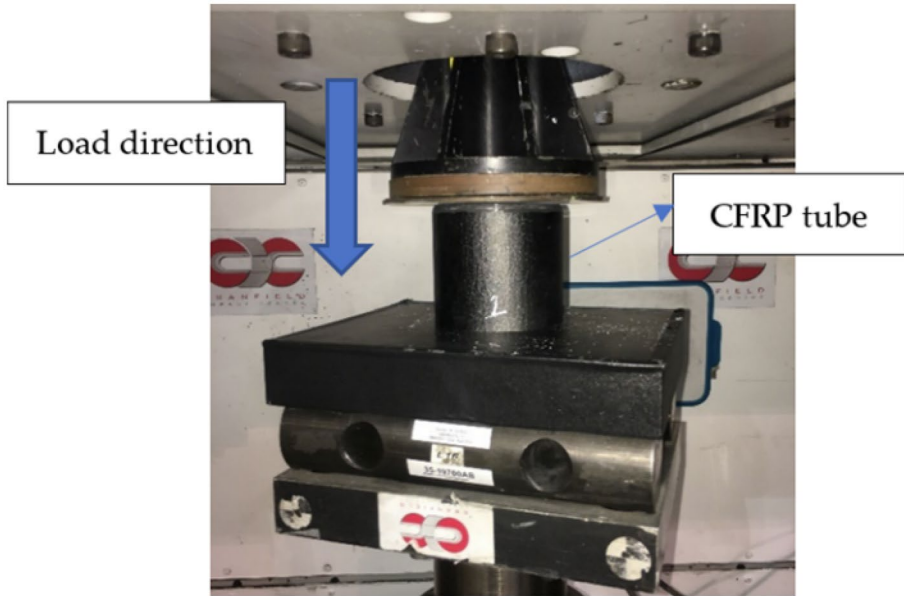

Fig. 1 Test sample geometry definition

Fig. 2 Experimental setup @Cranfield Impact Centre (CIC)

2.3 Test Results

The average force and velocity of the test are plotted against the displacement of the hammerhead as shown in Fig. 3. There are three different zones, starting with an initial almost linear part from point O to A, where the failure mechanism created by the trigger governs. After this, progressive crushing is observed between points A to B, in which the crushing process is stable and a high mean load is obtained. Finally, from points B to C there is an increase in the load because the debris accumulated in the main central crack, being this region of the graph is called the 'compaction zone'.

The main parameters of the impact studies are peak force (F_{max}), mean force (F_m), maximum displacement (d), Specific Energy Absorption (SEA) defined as the area under the force-displacement diagram and Crushing Force Efficiency (CFE) as the ratio between initial collapse force and mean crushing force are presented in Table 1.

The deformed shape of the impacted tubes is shown in Fig. 3. According to the test results, the failure mechanism is a mainly brittle fracture of the plies during the impact.

The internal and external fronds show both axial and transverse fragmentation in several locations, which also contribute to energy absorption. Both internal and external mid-walls of the tube are separated by the 'debris wedge'. This wedge is formed because of the Mode-I crack propagation. Some debris was produced during the impact which is

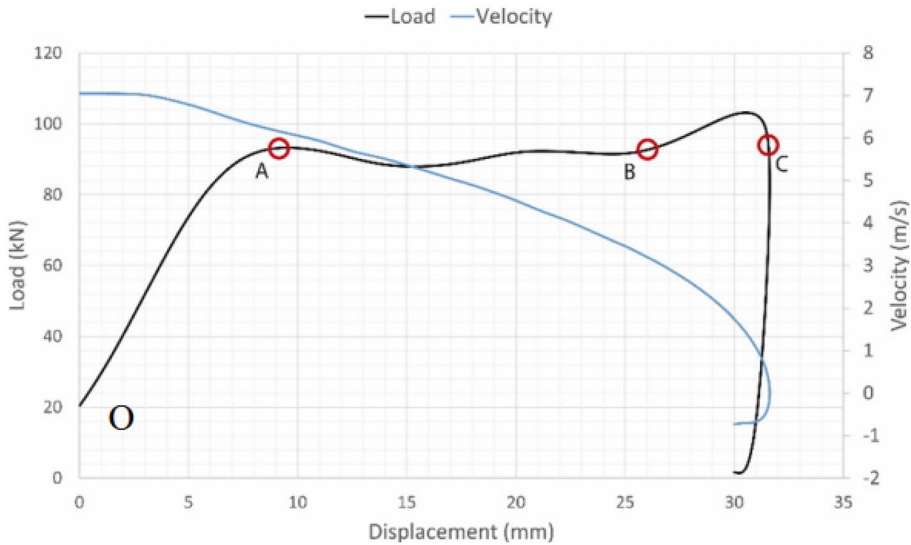|	$F_{max}(kN)$	$F_m(kN)$	$d(mm)$	$SEA(J/g)$	$CFE(\%)$
Table 1 Crashworthiness parameters from experimental results (3 tested specimens)	103 ± 2	89 ± 2	32 ± 1	58 ± 2	87 ± 2

Fig. 3 Average test results of experimental studies. (**A**) initial collapse load and maximum load (F_{max}), (**B**) mean force (F_m) and (**C**) final collapse

accumulated at the crack tip, and that is why this region is called a 'debris wedge'. In Figs. 4 and 5, the deformed bundles of −45° and 0° plies are presented in Fig. 4.

3 Numerical Modeling

The FE model of the experimental test is developed in LS-DYNA software. According to Rabiee and Ghasemnejad [21], the best way to model a CFRP tubular structure under impact is obtained with a double shell configuration. The mesh of the tube is defined by using Belytschko-Tsai with reduced integration circular shell elements applied to the same geometry similar to the experimental specimens, whereas the impactor is modelled as a rigid body, with a total mass of 108.4 kg by using a cubic geometry of $120 \times 120 \times 5$ mm³.
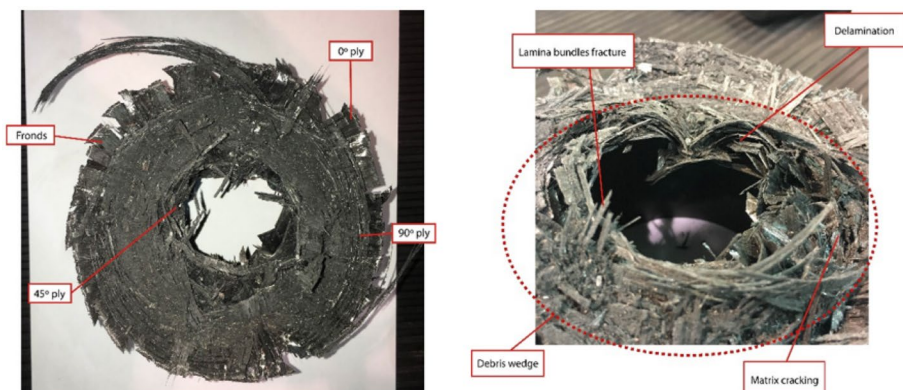
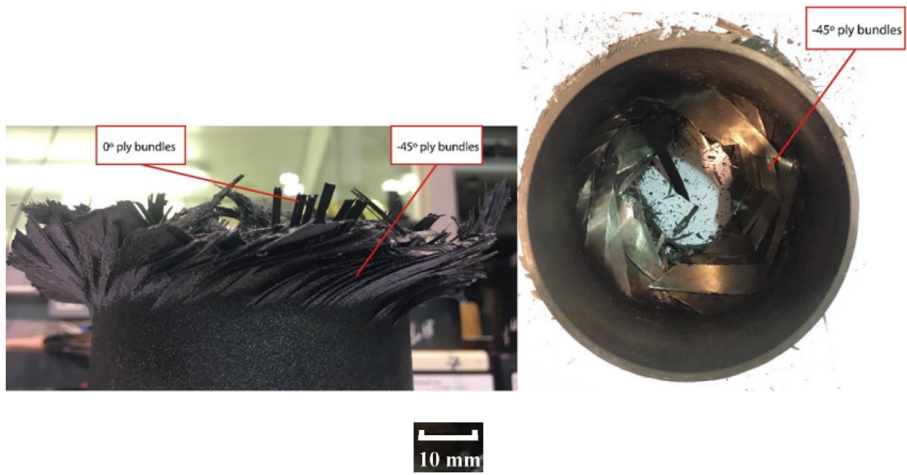**Fig. 4** Top and detailed view of tested specimen

Fig. 5 Side and bottom view of tested specimen

A mesh sensitivity analysis is conducted both in impactor and tube mesh size, reaching the conclusion that the results are mesh dependent, and selecting 3×3 elements in the tube, which ensures the right failure mechanisms without increasing the hourglassing. As for the boundary conditions, the bottom nodes of both inner and outer shells are pinned. An initial velocity of 7 m/s is defined in the impactor as shown in Fig. 6.

The thickness of the shell elements at the top of each tube is reduced from 1.43*mm* to 0.05*mm* to introduce a trigger mechanism to the composite tube. The material card *MAT54* which implements the Chang-Chang failure criterion was selected to model the composite damage model [20, 30, 31]. The material formulation is presented in LS-DYNA User's manual [36] and studied by Osborne et al. [37]. The elastic or constitutive properties are E_1, E_2, G_{12} and ν_{21} are taken from the datasheet of material in [38]. The constitutive properties and values of *MAT*54 parameters are presented in Table 2.

To correctly predict the progressive separation between both sub-laminates, *One_Way_Surface_To_Surface_Tiebreak* contact is defined, with Option 8 active. This is
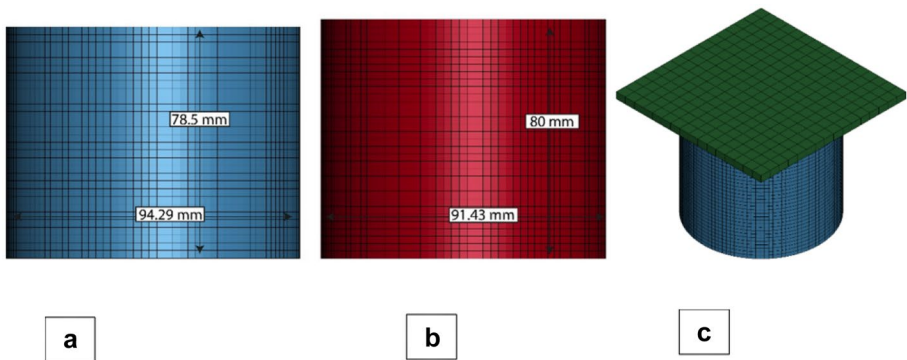

Fig. 6 The geometry of the FE Model. Inner Shell (Left), Outer Shell (Mid) and Assembly (Right). Two inner (**a**), outer (**b**) shells and (**c**) isometric view of striker and tube assembly

Table 2 MAT54, material properties values [38]

$E_1(GPa)$	$E_2(GPa)$	$G_{12}(GPa)$	v_{12}	$V_f(\%)$
119.3	8.2	3.6	0.34	60
DFAILM	*DFAILS*	*DFAILT*	*DFAILC*	*SOFT*
0.15	0.2	0.06	-0.06	0.8
XC(MPa)	*XT(MPa)*	*YC(MPa)*	*YT(MPa)*	*S(MPa)*
2200	2282	820	54	260

an energy-based contact card, which keeps both shells ended until a maximum normal (NFLS) or shear stress (SFLS) is reached. To formulate the friction between both shells, Coulomb friction is used to change from static to dynamic friction [32]. According to Rabiee and Ghasemnejad [20], in composite crushing simulations, Mode-I fracture is the dominant mode of failure, and the simplification of pure Mode-I delamination is reasonable. The tiebreak input parameters to the contact card are shown in Table 3, whereas static and dynamic friction coefficients are taken as 0.3 and 0.2 respectively.

The contact between the impactor and the CFRP tube is defined by using an Automatic_Nodes_To_Surface contact card, with static and dynamic friction coefficients of 0.3 and 0.2. The hourglass control method is chosen as a viscous form of hourglass control with a coefficient of 3%. A filter of 180 Hz filter is applied to the results in the same way as it was found in the experimental test.

The load-displacement curve obtained is shown in Fig. 7. An accurate prediction of the initial crushing is achieved, with a correct stiffness and initial peak value. After the initial peak, the drop in the curve is most important than in the experimental test, with a difference of 25% around 22*mm* displacements. The load value at the end of the analysis matches the experimental values. A difference of 18% is observed in the value of final displacement since the drop in the load value after the initial peak leads the tube to a lower energy absorption capability. The crashworthiness parameters are presented in Table 4.

In Fig. 8, the front and top view of the crushed tube is shown. The double-shell configuration does not predict the crushed shape, since the different layers are not modelled individually. The failure mechanism is based on ply brittleness and Mode-I fracture between both shells, and the petal formation is successfully predicted. Some element deletion is observed to obtain this petal formation. The difference between experimental and FE results in section a is related to the de-bouncing phenomenon of petals after deformations.

The Mode-I crack propagation is also predicted as can be seen in Fig. 9.

4 Z-Pinning

Since the main effect of the z-pins in the material is to increase the fracture toughness. An enhanced energy contact card can be defined at the reinforced zone to model the effect of the pins. This method has the drawback of not having a modifiable formulation and just the linear relationship that LS-DYNA or other software imposes on the energy-based

Table 3 Tiebreak inputs parameters in FE model

$G_{IC}(kJ/m^2)$	*NFLS(MPa)*	*SFLS(MPa)*	*PARAM(mm)*	*PARAMι(mm)*
0.2	25	55	0.016	0.08

Table 4 Comparison between experimental and numerical studies

	$F_{max}(kN)$	$F_m(kN)$	$d(mm)$	$SEA(J/g)$	$CFE(\%)$
Exp	103	89.6	32	58	87
FEM	102	58.3	37	49	84
Difference (%)	1.5	4.9	18	15	3.5

contact card. This approach has been used in the literature to model other through-the-thickness reinforcements in CFRP, such as stitching applied to CFRP tubes under axial impact, showing a good accuracy concerning experimental results [20, 31].

4.1 Reinforced Model Description

By analysing the available modelling techniques, the author decides to model the z-pinning reinforcement with an energy-based contact, since good results have been obtained in previous stitched models. Furthermore, because the interlaminar fracture was assumed to be pure Mode-I under the axial crushing impact, this energy-based contact was found sufficient to model z-pins. Because of time constraints, DCB and ENF tests could not be conducted, and an estimation of the enhanced fracture toughness is defined based on the literature data. According to Mouritz [27], for a volume content near 1, the value of G_{IC} is increased by 8 times, whereas G_{IIC} value is increased by 3 times. In the same way for the unpinned model, pure Mode-I interlaminar fracture is assumed. Two different zones are defined in the One_Way_Surface_To_Surface_Tiebreak contact: a reinforced zone, with the same tiebreak definition as in the unpinned model; and a reinforced zone, where G_{IC} is increased by 8 times by increasing the PARAM value with NFLS and SFLS constants. A DCB test simulation is
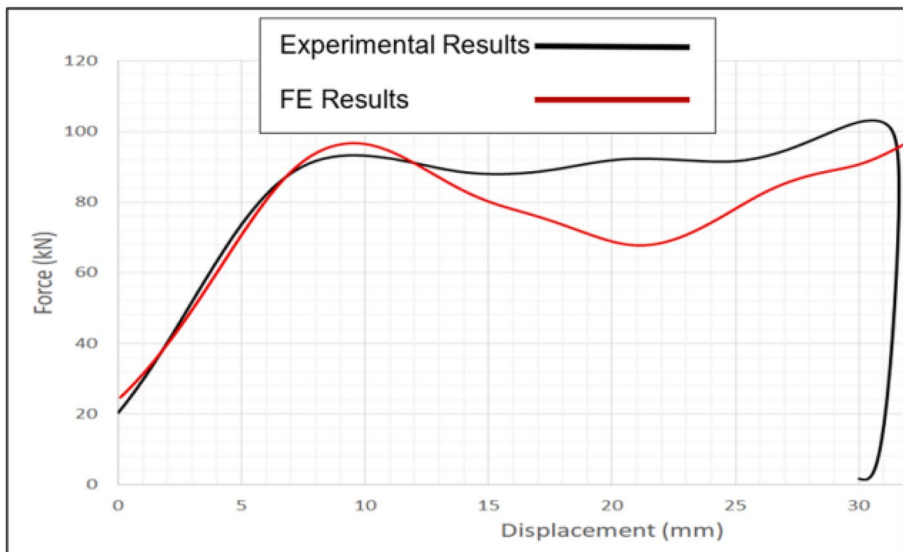
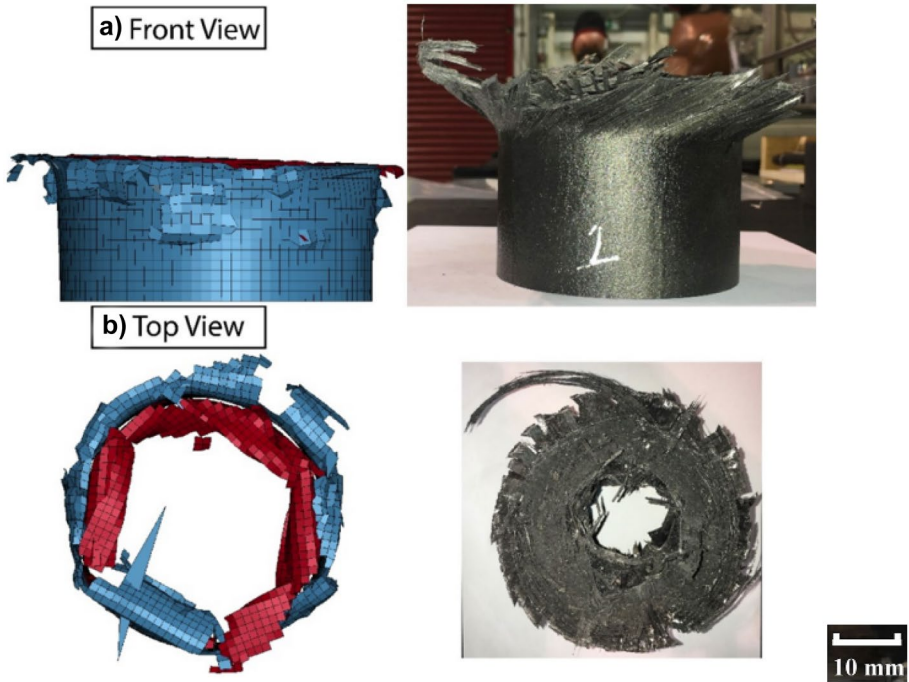**Fig. 7** Comparison between experimental and FE results

Fig. 8 Comparison between FEM and experimental crushed morphologies

conducted for both unpinned and z-pinned tiebreak parameters. In Fig. 10, both deformed shapes at the end of the simulation are shown, as well as the load-displacement curve. The reinforced model has a higher load carrying capacity, with a higher displacement applied
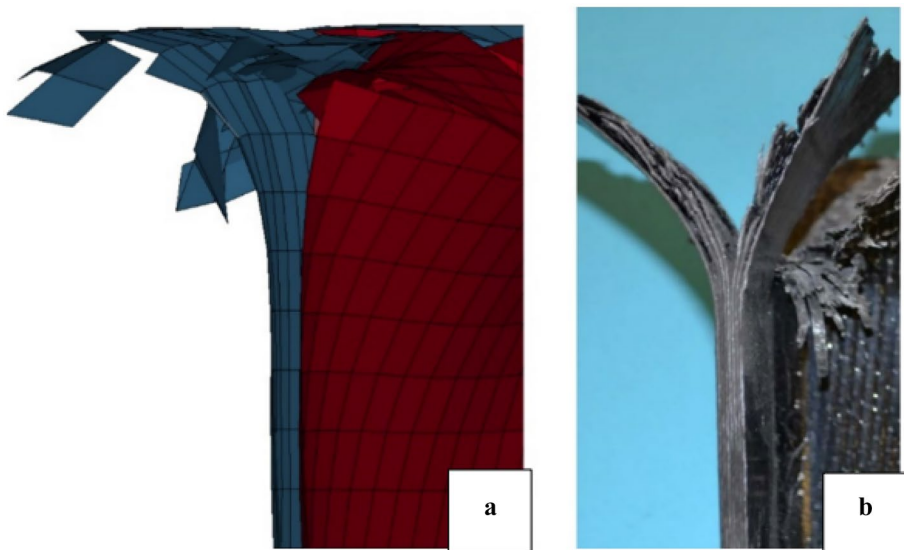

Fig. 9 Mode-I interlaminar crack propagation, (**a**) FEM and (**b**) Experimental results
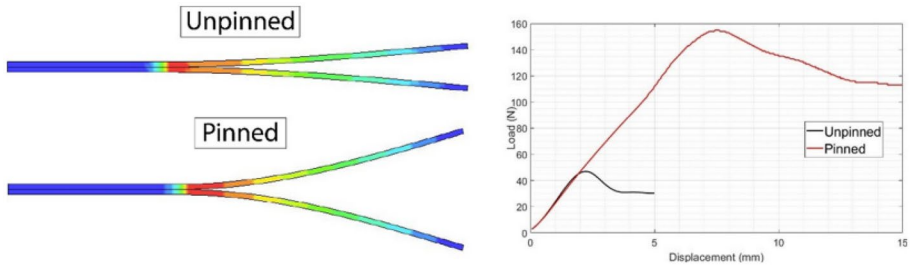
Fig. 10 Comparison of DCB deformed shape (left) and load-displacement curves (right)

until the crack propagates. The curve is similar to the experimental results obtained by Cartié and Partridge [24].

4.2 Z-pins Pattern Designs

Five different designs of z-pinned CFRP tubes are proposed, which are shown in Fig. 11.

Uniform: A rectangular band with the same pin volume content, i.e., with the same increase in G_{IC} value. The band is applied at a distance of 6 mm from the top of the specimen to obtain a progressive crushing. Horizontal banded: Three different bands with the same height are reinforced. All bands have the same pin volume content. Vertical banded: Vertical strips of the same width and height are reinforced with the same pin volume content. Increased: A rectangular band is reinforced but by increasing pin volume content. Thus, three different bands are defined: the first one with $G_{IC} = (8/3)G_{ICUNP}$, the second one with $G_{IC} = (16/3)G_{ICUNP}$ and the third one with $G_{IC} = 8G_{ICUNP}$. Decreased: The same basis as 'Increase' is followed, however, the bands have a decreasing pin volume content.
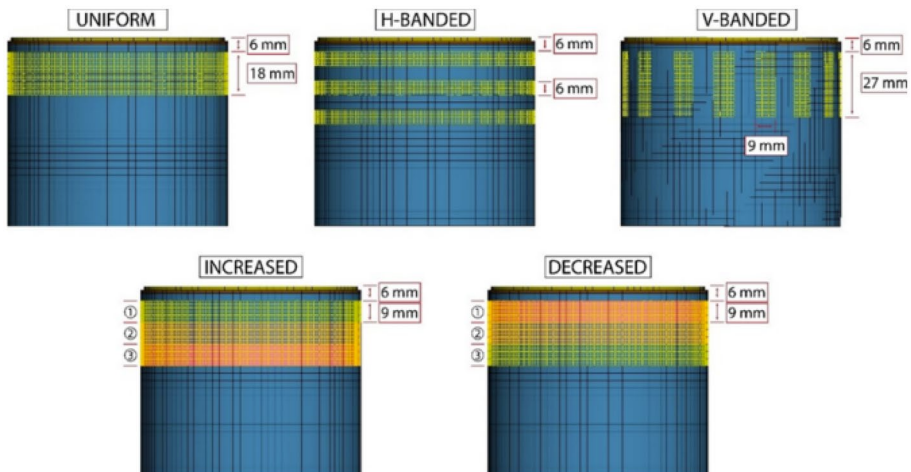

Fig. 11 Proposed reinforced designs of z-pinned specimens

5 Results and Discussion

The results obtained for each design are presented and compared with the unpinned design. To help the reader easily differentiate the results, the curves and crushed morphologies have been split into two Figs. 12, 13 and 14. The 'uniform' design reduces the drop after the initial peak in comparison with the unpinned design, and the compaction zone is less significant. In the crushed morphology, higher ply bending is observed in the initial stages of the impact (see detail in Fig. 12), although the most important failure mechanism still is the petal formation and ply brittleness.

The 'horizontal banded' design leads to a progressive crushing which does not show a significant drop after the initial peak, which is a better result in terms of crashworthiness. On the other hand, the 'vertical banded' shows the same initial drop similar to unpinned design, although the final compaction zone is not as significant. Both banded designs show good failure mechanisms during the whole analysis, even with less ply bending in comparison with unpinned design.

The 'increased' and 'decreased' designs show behaviour which is, in shape as was expected. Therefore, the 'increased' model shows a lower initial strength at the beginning of the analysis, and it rises when the impact advances. On the other hand, the 'decreased' design shows a higher initial peak at the beginning, and a progressive reduction of the strength when the impact advances. As for the crushing process shapes, the 'increased' design shows higher ply failure at the bottom of the tube (see detail 1 in Fig. 14), and ply bending is observed in the 'decreased' design (see detail 2 in Fig. 14).

It can be concluded that a higher increase of the G_{IC} value at the top of the specimen, such as in 'uniform' and 'decreased' designs, leads to a ply bending failure mechanism, whereas other designs show a better progressive petal formation.

The crashworthiness parameters are presented in Table 5. The maximum force is reduced in all the designs concerning the unpinned tube since this maximum force is
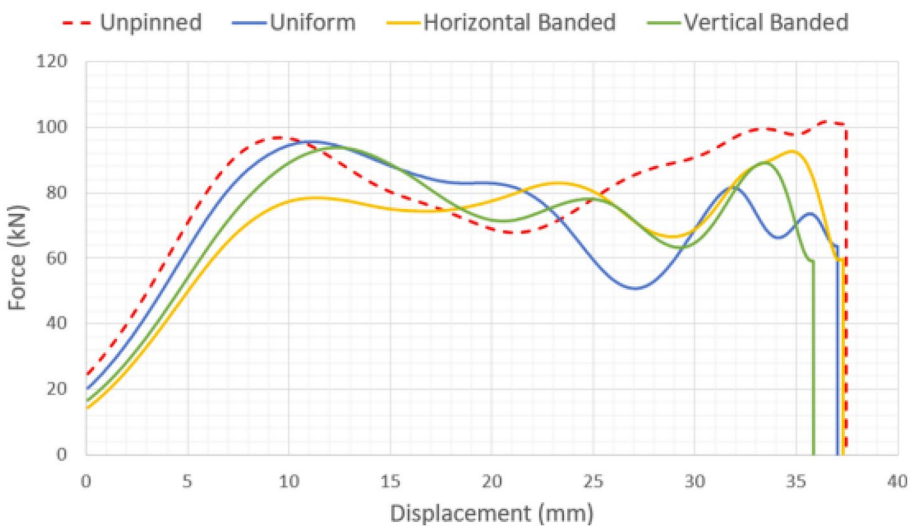

Fig. 12 Comparison of load-displacement curves, z-pin designs (I)
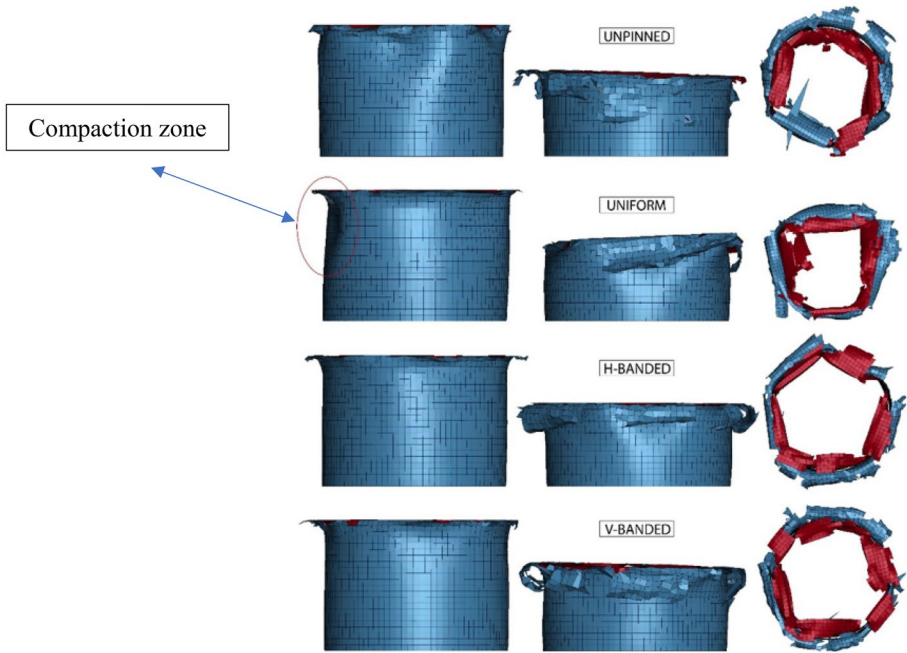
Compaction zone

Fig. 13 Z-pinned crushed morphologies (I)

reached in the compaction zone, not in the initial peak. The 'horizontal banded' has a lower initial peak which shows a lower maximum force at the end.

The highest value of mean load was observed in the unpinned design, while the minimum mean load was obtained in the 'decreased' design (21.98% lower than unpinned).
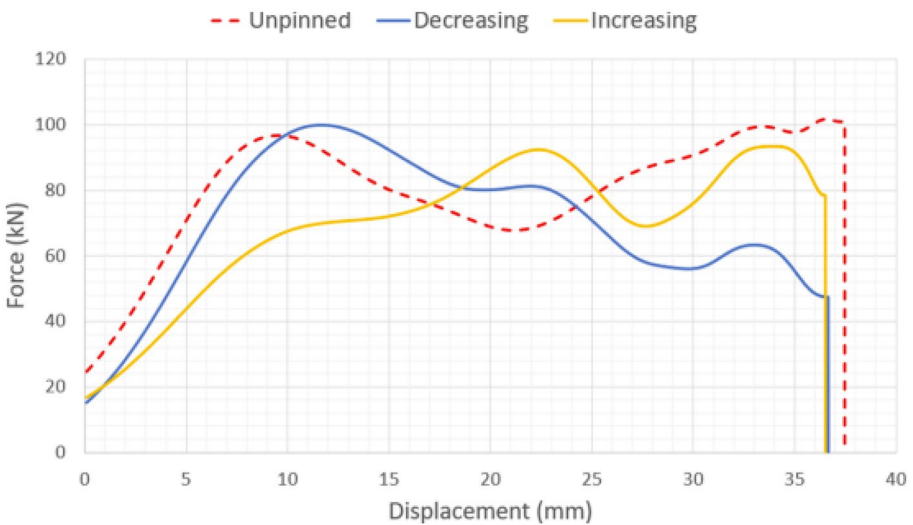

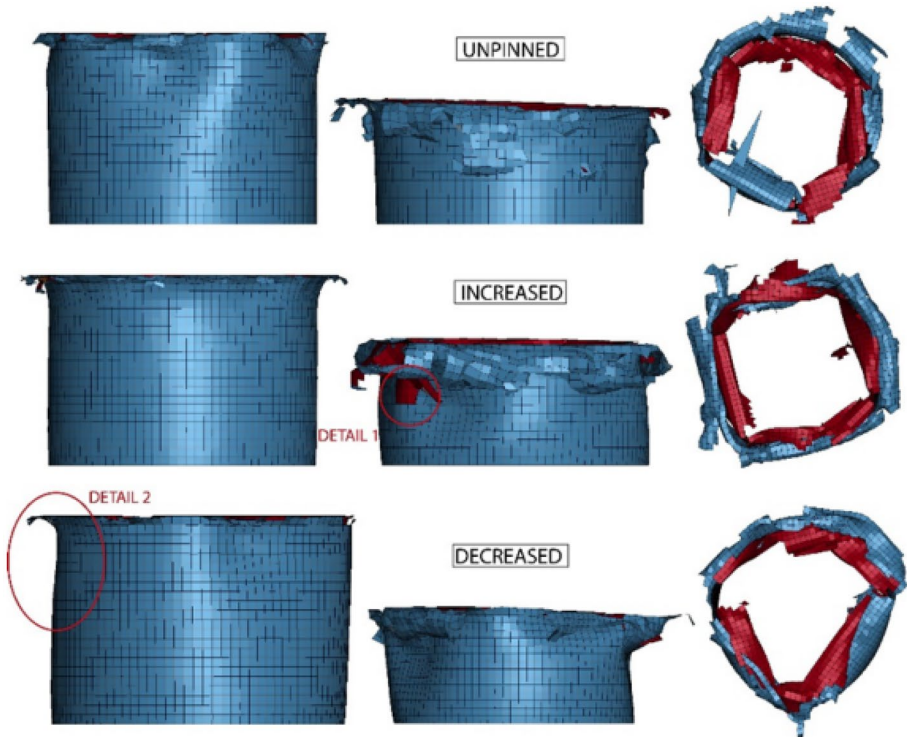**Fig. 14** Comparison of load-displacement curves, z-pin designs (II)

Fig. 15 Z-pinned crushed morphologies (II)

However, the values of SEA are similar, being the optimum the 'vertical banded' design (4.49% higher than unpinned), followed by the 'increased' design (2.61%). The highest value of CFE is obtained with the unpinned model, followed by the 'increased' design, and the least value of CFE is assigned to the 'decreased' design (see Fig. 15).

6 Conclusions

This study has focused on the z-pin reinforcing technique applied to CFRP tubes under axial impact, to maximize the SEA value and have an enhanced crashworthiness performance. The following facts have been concluded from this study.

1. Manufacturing and experimental testing of unpinned tubes were successfully conducted, analysing the results, and developing deep knowledge about the failure mechanism which absorbs energy during the impact. The experimental data was used to validate numerical results.
2. A numerical model based on double-shell configuration was developed in LS-DYNA, by performing a deep parametric study, mesh sensitivity analysis and trigger mechanism study.
3. The model has been validated, with good failure mechanism prediction, and with a maximum error of 10% (see Fig. 7). Our results indicate that z-pinning improves the

Table 5 Comparison of crashworthiness parameters for various z-pinned designs

	$F_{max}(kN)$	$F_m(kN)$	$d(mm)$	$SEA(J/g)$	$CFE(\%)$
Unpinned	101	85	37	49	84
Uniform	95	71	37	50	75
H-Band	96	73	37	50	76
V-Band	94	73	37	52	77
Increased	93	75	37	51	81
Decreased	100	67	37	51	67

SEA in all designs and reduces initial collapse load in comparison with the unpinned samples (see Table 5).

4. Current z-pinning modelling techniques have been researched, and an enhanced energy-based contact has been used to model the z-pin reinforcement. Five different designs have been studied.

5. The 'Vertical banded' design shows the highest SEA and least initial collapse load values in comparison with the unpinned specimen, which indicates an improvement in crashworthiness parameters of z-pinned composite tubes.

6. The V-banded design allows the formation of axial cracks between the pinned areas. This phenomenon reduces the initial resistance of the composite tube against the load at the beginning of the crushing process and leads to a lower initial collapse load in comparison with other designs [3, 23].

Declarations

References

1. Bisagni, C.: Experimental investigation of the collapse modes and energy absorption characteristics of composite tubes. Int. J. Crashworthiness. **14**(4), 365–378 (2009). https://doi.org/10.1080/13588260902792954

2. Rabiee, A., Ghasemnejad, H.: Progressive Crushing of Polymer Matrix Composite Tubular Structures: Review. Open J. Compos. Mater. **07**(01), 14–48 (2017). https://doi.org/10.4236/ojcm.2017.71002

3. Marc, A.: Courteau. Investigating the Crashworthiness Characteristics of Carbon Fiber/Epoxy Tubes. (December). (2011)

4. Cauchi Savona, S., Hogg, P.J.: Effect of fracture toughness properties on the crushing of flat composite plates. Compos. Sci. Technol. **66**(13), 2317–2328 (2006). https://doi.org/10.1016/j.compscitech.2005.11.038

5. Ghasemnejad, H., Blackman, B.R.K., Hadavinia, H., Sudall, B.: Experimental studies on fracture characterisation and energy absorption of GFRP composite box structures. Compos. Struct. Elsevier Ltd. **88**(2), 253–261 (2009). https://doi.org/10.1016/j.compstruct.2008.04.006

6. Ghasemnejad, H., Hadavinia, H.: Off-axis crashworthiness characteristic of woven glass/epoxy composite box structures. J. Reinforced Plastics Compos. **29**(15), 2306–2330 (2010). https://doi.org/10.1177/0731684409347807

7. Hadavinia, H., Ghasemnejad, H.: Effects of Mode-I and Mode-II interlaminar fracture toughness on the energy absorption of CFRP twill/weave composite box sections. Compos. Struct. Elsevier Ltd. **89**(2), 303–314 (2009). https://doi.org/10.1016/j.compstruct.2008.08.004

8. Ghasemnejad, H., Hadavinia, H., Aboutorabi, A.: Effect of Delamination Failure in Crashworthiness Analysis of Hybrid Composite box Structures. Materials and Design, **31**, 1105–1116. Elsevier Ltd (2010). https://doi.org/10.1016/j.matdes.2009.09.043

9. Tong, L., Mouritz, A.P., Bannister, M.K.: 3D Fibre Reinforced Polymer Composites. (2002)

10. Aoki, Y., Yosuke, N., Takashi, I.: Experimental evaluation and consideration of numerical method of zanchor CFRP laminates.Advanced Composite Technology Center, Japan Aerospace Exploration Agency. 1–2. (2006)

11. Korkiakoski, S., Sarlin, E., Suihkonen, R., Saarela, O.: Influence of reinforcement positioning on tension-tension fatigue performance of quasi-unidirectional GFRP laminates made of stitched fabrics. Compos. Part B: Eng. **112**, 38–48 (2017). https://doi.org/10.1016/j.compositesb.2016.12.017 Elsevier Ltd. Disponible en

12. Mouritz, A.P., Cox, B.N.: Mechanistic approach to the properties of stitched laminates. Compos. Part A: Appl. Sci. Manufac. **31**(1), 1–27 (2000). https://doi.org/10.1016/S1359-835X(99)00056-1

13. Yasaee, M., Bigg, L., Mohamed, G., Hallett, S.R.: Influence of Z-pin embedded length on the interlaminar traction response of multi-directional composite laminates. Mater. Design. **115**, 26–36 (2017)

14. Ghafari-Namini, N., Ghasemnejad, H.: Effect of Natural Stitched Composites on the Crashworthiness of box Structures. Materials and Design, **39**, 484–494. Elsevier Ltd (2012). https://doi.org/10.1016/j.matdes.2012.03.025

15. Rabiee, A., Ghasemnejad, H.: Effect of multi stitched locations on high speed crushing of composite tubular structures. Compos. Part B: Eng. Elsevier Ltd. **100**, 164–175 (2016). https://doi.org/10.1016/j.compositesb.2016.06.068

16. Lander, J.K.: Designing with z-pins: locally reinforced composite structures. (2008). http://hdl.handle.net/1826/4072

17. Cartié, D.D.R., Partridge, I.K.: Delamination behaviour of Z-pinned laminates. European Structural Integrity Society. **27**(C), 27–36 (2000). https://doi.org/10.1016/S1566-1369(00)80005-9

18. Rugg, K.L., Cox, B.N., Massabò, R.: Mixed mode delamination of polymer composite laminates reinforced through the thickness by z-fibers. Compos. - Part A: Appl. Sci. Manuf. **33**(2), 177–190 (2002). https://doi.org/10.1016/S1359-835X(01)00109-9

19. Partridge, I.K., Cartié, D.D.R.: Delamination resistant laminates by Z-Fiber® pinning: Part I manufacture and fracture performance. Compos. Part A: Appl. Sci. Manufac. **36**(1), 55–64 (2005). https://doi.org/10.1016/j.compositesa.2004.06.029

20. Mouritz, A.P., Cox, B.N.: Mechanistic approach to the properties of stitched laminates. Composites Part A: Applied Science and Manufacturing. 31(1), 1–27 (2000). https://doi.org/10.1016/S1359-835X(99)00056-1

21. Rabiee, A., Ghasemnejad, H. Lightweight design to improve crushing behaviour of multi-stitched composite tubular structures under impact loading. Thin-Walled Structures. Elsevier Ltd. 135(August 2018), 109–122 (2019). https://doi.org/10.1016/j.tws.2018.11.002

22. Ghafari-Namini, N., Ghasemnejad, H.: Effect of natural stitched composites on the crashworthiness of box Structures. Mater. Des. **39**, 484–494 (2012). https://doi.org/10.1016/j.matdes.2012.03.025

23. Lander, J.K.: Designing with z-pins: locally reinforced composite structures. (2008). Disponible en: http://hdl.handle.net/1826/4072

24. Cartié, D.D.R., Partridge, I.K.: Delamination behaviour of Z-pinned laminates. European Structural Integrity Society. **27**(C), 27–36 (2000). https://doi.org/10.1016/S1566-1369(00)80005-9

25. Mouritz, A.P.: Review of z-pinned composite laminates. Composites part. Appl. Sci. Manuf. **38**(12), 2383–2397 (2007). https://doi.org/10.1016/j.compositesa.2007.08.016

26. Dickinson, L.C., Farley, G.L., Hinders, M.K.: Prediction of effective three-dimensional elastic constants of translaminar reinforced composites. Hispanic J Behav Sci. 183–205 (1999)

27. Chang, P., Mouritz, A.P., Cox, B.N.: Properties and failure mechanisms of z-pinned laminates in monotonic and cyclic tension. Compos. Part A: Appl. Sci. Manufac. **37**(10), 1501–1513 (2006). https://doi.org/10.1016/j.compositesa.2005.11.013

28. Mengjia, L., Puhui, C.: A new FE model for predicting the binding micromechanisms of a Z-pin. (2019)

29. Blacklock, M., Joosten, M., Zeineddine, A., Mouritz, A.: Efficient finite element modelling of Z-pin reinforced composites using the binary model. ICCM International Conferences on Composite Materials. 2015, 19–24 (2015)

30. Bianchi, F., Koh, T.M., Zhang, X., Partridge, I.K., Mouritz, A.P.: Finite element modelling of z-pinned composite T-joints. Compos. Sci. Technol. **73**(1), 48–56 (2012). https://doi.org/10.1016/j.compscitech.2012.09.008

31. Liu, Y., Cai, L., Ding, H., Xu, Q.: Out-of-plane Properties and Failure Mechanism of Composite Laminates Reinforced With Carbon Z-pins, Applied Composite Materials. **30**, 379–397 (2023). https://doi.org/10.1007/s10443-022-10087-4

32. Knopp, A., Scharr, G.: Compression properties of z-pinned carbon-fibre/epoxy laminates reinforced with circumferentially notched z-pins. Compos. Sci. Technol. **201**, 108486 (2021). https://doi.org/10.1016/j.compscitech.2020.108486

33. Liao, B., Zhou, J., Zheng, J., Tao, R., Xi, L., Zhao, T., Li, Y., Fang, D.: Effect of Z-pin inclined angle on the impact damage suppression effectiveness for cross-ply composite laminates. Compos. Pt A-Appl Sci. Manuf. **142**, 106264 (2021). https://doi.org/10.1016/j.compositesa.2020.106264

34. Rabiee, A., Ghasemnejad, H.: Laminate Tailoring of Composite Tubular Structures to improve Crashworthiness Design at Off-Axis Loading. Open J. Compos. Mater. **08**(03), 84–109 (2018). https://doi.org/10.4236/ojcm.2018.83008

35. Rabiee, A., Ghasemnejad, H.: Improvement of specific energy absorption of Composite Tubular Absorbers using various stitching pattern designs. Appl. Compos. Mater. Springer Neth. **27**(6), 717–738 (2020). https://doi.org/10.1007/s10443-020-09842-2

36. Livermore Software Technology Corporation: L{S}-{DYNA} - {K}eyword {U}ser's {M}anual, Version 970. (2003)

37. Osborne, M.: Single-Element Characterization of the LS-DYNA MAT54 Material Model. The University of Washington (2012)

38. SHD Composites. VTC401 Epoxy Component Prepreg. (February):1–3 (2018). http://shdcomposites.com/wp-content/uploads/2016/03/MTC801-TDS.pdf

2023-05-23

Z-pinning techniques to improve energy absorption capabilities of CFRP tubular structures

Ramírez, J. G.

Springer